JURNAL KIMIA VALENSI
p-ISSN: 2460-6065; e-ISSN: 2548-3013
Journal homepage: https://journal.uinjkt.ac.id/index.php/valensi
Research Article

Copper-Supported Crosslinked Chitosan–Glutaraldehyde/Zinc Oxide: Interfacial Structure, Cyclic Voltammetric Behavior, and Reproducibility

Anceu Murniati [1,2*], Restu Muchammad Ibrahim[1,2], Intan Mulya Ewangga[1], Rolan Rusli[3]

[1]*Study Program of Master of Chemistry, Faculty of Sciences and Informatics, Universitas Jenderal Achmad Yani, Jl. Terusan Jenderal Sudirman, Cimahi, 40531, Indonesia*
[2]*Material and Environmental Development Centre, Universitas Jenderal Achmad Yani, Jl. Terusan Jenderal Sudirman, Cimahi, 40531, Indonesia*
[3]*Pharmaceutical Chemistry Division, Faculty of Pharmacy, Mulawarman University, Jl. Penajam, Kampus Unmul Gn. Kelua, Samarinda, Kalimantan Timur, 75119, Indonesia*

[*]*Email: anceu.murniati@lecture.unjani.ac.id*

Article Info
Received: Sept 10, 2025
Revised: Marc 28, 2026
Accepted: Apr 19, 2026
Online: May 31, 2026

Citation:
Murniati, A., Ibrahim, R. M., Ewangga, I. M., Rusli, R. (2026). Copper-Supported Crosslinked Chitosan–Glutaraldehyde/Zinc Oxide: Interfacial Structure, Cyclic Voltammetric Behavior, and Reproducibility. *Jurnal Kimia Valensi*, 12(1), 49-63.

Doi: 10.15408/jkv.v12i1.46454

Abstract

Chitosan-based nanocomposite coatings are promising low-cost electrochemical materials, but the relationship between interfacial structure and voltammetric performance remains insufficiently understood. This study investigated the cyclic voltammetric behavior, reproducibility, and cycling stability of a copper-supported crosslinked chitosan–glutaraldehyde/zinc oxide coating. Structural and electrochemical characterization was performed using Fourier transform infrared spectroscopy, scanning electron microscopy/energy-dispersive X-ray spectroscopy, and cyclic voltammetry in 0.1 M phosphate-buffered saline and 0.01 M $K_3[Fe(CN)_6]$/0.10 M KCl. The coating showed Schiff-base crosslinking, Zn-related interactions, compact morphology, good attachment to copper, and distributed Zn-containing domains without obvious large-scale agglomeration. Electrochemically, the coating exhibited quasi-reversible behavior in both media. Ferricyanide produced sharper redox features, current ratios closer to unity, and stronger anodic linearity with the square root of scan rate than phosphate-buffered saline. The apparent diffusion coefficient estimated from the ferricyanide anodic response was on the order of 10^{-5}–10^{-6} cm² s^{-1}. Reproducibility across ten independently prepared electrodes was acceptable, with lower variability in ferricyanide than in phosphate-buffered saline, and the voltammetric profile was retained over 15 cycles. These results demonstrate a stable and reasonably reproducible electrochemical interface with potential for future sensing applications.

Keywords: Cyclic voltammetry, diffusion-controlled electron transfer, interfacial structure, reproducibility, zinc oxide–crosslinked chitosan coating

1. INTRODUCTION

Electrochemical sensors have attracted increasing attention because they combine simple fabrication, low cost, operational stability, and high sensitivity. Advances in this field have been strongly supported by the development of modified electrodes, including nanostructured surfaces and electrodeposited architectures, which have shown promising performance in formaldehyde detection and other catalytic applications [1–4]. In parallel, nanocomposite materials have emerged as efficient catalytic platforms for formaldehyde oxidation and related electrochemical processes [5,6]. These developments highlight the importance of designing electrode coatings that not only improve electrochemical response but also offer structural stability and reproducibility.

Among polymeric materials, chitosan (CS) is particularly attractive as a matrix for electrochemical applications because it is abundant, environmentally friendly, and capable of providing rapid response, low cost, and good repeatability [7,8]. In addition, chitosan is widely recognized as a biodegradable, biocompatible, and non-toxic biopolymer derived from renewable

resources, with broad potential in biomedical and biosensing applications, further supporting its relevance as a functional material for electrochemical interface design.[9,10]

Its biocompatibility, porosity, hydrophilicity, and rich –OH/–NH_2 functionality make CS an attractive thin-film matrix for electrochemical interfaces[11–13], while chemical/structural modification can tune pore architecture, mechanical resistance, stability, and adsorption/desorption behavior[14]. However, the practical use of CS films remains limited by their relatively brittle nature and the need for improved structural durability under repeated electrochemical operation.

To overcome these limitations, hybridization and crosslinking strategies have been widely explored. CS–metal-oxide hybrids have shown broad utility, for example, Fe_3O_4–CS for protein biosensing[15], CS/ZnO for glucose detection[16], CS–Zn nanoparticles for immunosensing[12], and CuO–CS as a glassy-carbon modifier[17]. To address the brittleness and enhance structural stability of CS films, crosslinkers are commonly introduced[18], and among them, glutaraldehyde (GLA) is one of the most widely used because it strengthens the polymer network, improves film durability, and can enhance selectivity and sorption behavior in CS-based materials[19–21]. Zinc oxide (ZnO), intensively studied since the 1960s, supports sensing, transduction, and catalysis[22]. When incorporated into CS, ZnO can enhance mechanical strength and introduce Lewis-acidic Zn^{2+} centers that interact with donor sites in the polymer matrix[23]. Related advances include Cu-doped ZnO formaldehyde sensors[4], CS-GLA/Fe_3O_4 composites with ZnO for dye adsorption[24], and CS–ZnO nanocomposites with antibacterial, photocatalytic, and hydrophobic properties for food-related hazard detection[23]. Elongation tests showed that in situ–incorporated ZnO nanoparticles markedly strengthened CS films, improving extensibility and durability[25].

Cyclic voltammetry (CV) remains a versatile probe of mechanisms, electron transfer, catalysis, and kinetics across inorganic and organic systems[26,27]. CV-based platforms have been widely applied in formaldehyde biosensing, with reported limits of detection in the range of 0.01–0.50 mg L^{-1}. [28] Although copper (Cu) is inexpensive and widely available, bare Cu often suffers from high overpotentials, limited selectivity, and oxidative instability[29,30]. Polymer modification helps overcome these drawbacks, with success demonstrated in drug detection[31] and composite membrane-based biosensors[32–34]. Despite these advances and the broader promise of composite systems in electrochemical applications[35,36], there remains a need for simple, robust, and low-cost coated electrodes with well-characterized interfacial structure and reproducible electrochemical behavior.

In this context, the present work focuses on a copper-supported crosslinked chitosan–glutaraldehyde/zinc oxide coating as a model electrochemical interface. Rather than directly claiming analyte-specific sensing performance, this study aims to clarify how interfacial chemistry and morphology are related to cyclic voltammetric behavior, cycling stability, and reproducibility. A chitosan–glutaraldehyde/zinc oxide nanocomposite film was fabricated on copper and characterized using Fourier transform infrared (FTIR) spectroscopy[37,38], scanning electron microscopy/energy-dispersive X-ray spectroscopy (SEM/EDS), and cyclic voltammetry in two electrolytes, namely 0.1 M phosphate-buffered saline (PBS, pH 7.0) and the ferri/ferrocyanide redox couple, $Fe(CN)_6^{3-/4-}$, in 0.10 M KCl. By correlating chemical structure, morphology/composition, and scan-rate-dependent electrochemical response, this work aims to establish a clearer structure–function relationship and provide a robust baseline for future electrochemical sensing applications based on chitosan-derived nanocomposite coatings.

2. RESEARCH METHODS

Materials

Chitosan (CS, 200–300 mesh) was prepared from blue crab shells (*Portunus pelagicus*) and used as the polymer matrix in this study, following our previously reported chitosan-based membrane preparation procedure.[39] Analytical-grade chemicals were used without further purification. Zinc oxide (ZnO) nanopowder (<100 nm, ≥99%), glutaraldehyde (GLA, 25% in H_2O), disodium hydrogen phosphate (Na_2HPO_4), sodium dihydrogen phosphate monohydrate ($NaH_2PO_4 \cdot H_2O$), potassium chloride (KCl, ≥99%), potassium ferricyanide ($K_3[Fe(CN)_6]$, 99%), phosphoric acid (H_3PO_4, 85%), and sodium hydroxide (NaOH, ≥97%) were purchased from Sigma-Aldrich. All solutions were prepared using deionized water (resistivity ≥18 MΩ·cm at 25 °C).

Equipment and instruments

Routine procedures were carried out using standard laboratory glassware. The instruments used in this study included an analytical balance (Mettler AE-200), pH meter (Hanna Checker), magnetic stirrer, ultrasonic cleaner (Branson 3510), potentiostat (Ingsen 1001), Fourier transform infrared (FTIR) spectrometer (Shimadzu Prestige-21), and scanning electron microscope/energy-dispersive X-ray spectroscopy (SEM/EDS) system (JEOL JSM-6510LA). Electrochemical measurements were conducted at the Chemistry Research Laboratory, Universitas Jenderal Achmad Yani (UNJANI), while FTIR and SEM/EDS characterizations were

performed at the Basic Science Laboratory, Institut Teknologi Bandung (ITB). All measurements were carried out under the standard operating conditions of the respective instruments.

Electrode preparation

High-purity copper strips (5.0 cm × 0.5 cm × 0.2 mm) were sequentially polished (SiC grit 1000 → 2000) and ultrasonically cleaned in ethanol and deionized water (5 min each). The electroactive area was masked to 0.90 cm^2. The chitosan–glutaraldehyde/zinc oxide (CS–GLA/ZnO) casting dispersion was prepared by dissolving chitosan (CS, 2.0% w/v) in 1% (v/v) acetic acid under continuous stirring until a homogeneous solution was obtained. Zinc oxide (ZnO, 0.6% w/v) was then added, followed by ultrasonication for 30 min to improve dispersion. After that, glutaraldehyde (GLA) was added as the crosslinking agent at 10% (v/v) relative to the total dispersion volume, using the 25% aqueous stock solution, and the mixture was stirred for 12 h at 25 °C at 100–300 rpm.

An aliquot of 20 µL of the resulting dispersion was drop-cast onto the masked copper surface and dried under ambient conditions to form the coating layer. The overall drop-casting procedure and integration of the coated copper electrode into the three-electrode electrochemical system are illustrated in **Figure 1.**

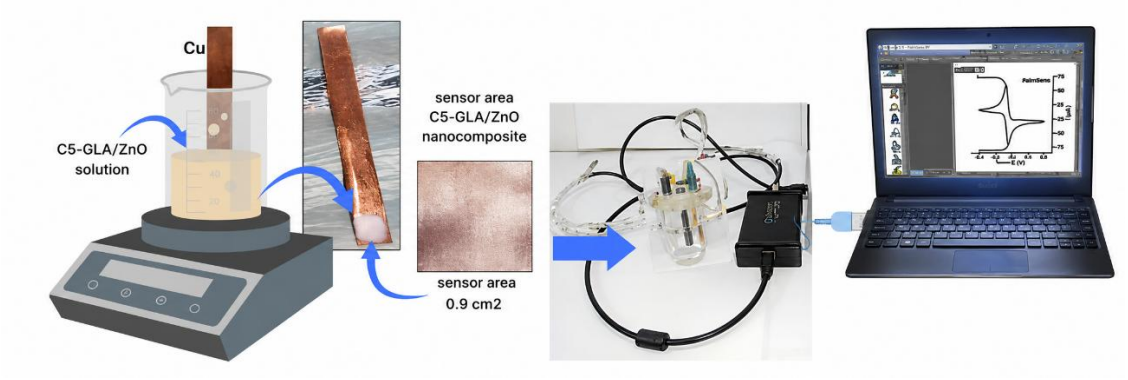

Figure 1. Schematic illustration of CS–GLA/ZnO coating fabrication on Cu by drop-casting and its integration into a three-electrode cyclic voltammetry setup

Electrochemical measurements (cyclic voltammetry)

Cyclic voltammetry (CV) measurements were performed in a 25 mL electrochemical cell using a conventional three-electrode configuration consisting of the copper-supported chitosan–glutaraldehyde/zinc oxide electrode (Cu|CS–GLA/ZnO) as the working electrode (WE), a Pt wire as the counter electrode (CE), and an Ag/AgCl (3 M KCl) electrode as the reference electrode (RE). The experiments were carried out under a nitrogen atmosphere at 25 ± 1 °C using an Ingsen 1001 potentiostat. Electrochemical data were processed using Origin 2024 and Microsoft Excel[37,40].

Two electrolyte systems were employed: (i) 0.1 M phosphate-buffered saline (PBS, pH 7.0) and (ii) 0.01 M $K_3[Fe(CN)_6]$ in 0.10 M KCl. Unless otherwise stated, the potential window was set from −1.0 to +1.0 V versus Ag/AgCl, and the scan rate was varied from 25–100 mV s^{-1}.

From each cyclic voltammogram, the anodic and cathodic peak currents (I_{pa} and I_{pc}), anodic and cathodic peak potentials (E_{pa} and E_{pc}), peak-to-peak separation (ΔE_p), and formal potential $E^{0\prime}$ = (E_{pa} + E_{pc})/2 were determined to evaluate electrochemical response, charge-transfer characteristics, and kinetic behavior. The apparent diffusion coefficient was estimated from the Randles–Ševčík relationship based on the dependence of peak current on the square root of scan rate.

Materials characterization

The morphology and thickness of the coating were examined using scanning electron microscopy/energy-dispersive X-ray spectroscopy (SEM/EDS; JEOL JSM-6510LA). Top-view SEM images were obtained at magnifications of 50×, 500×, 1500×, and 5000×, while cross-sectional observations were performed at 100× and 2000×. EDS spectra and elemental mapping were acquired at an accelerating voltage of 15 kV. The EDS results were treated as semi-quantitative, whereas elemental mapping was used to assess the spatial distribution and uniformity of Zn and O within the CS–GLA matrix.

Functional groups and interfacial chemical interactions in the coating were analyzed using Fourier transform infrared (FTIR) spectroscopy (Shimadzu Prestige-21). FTIR analysis was used to identify the characteristic absorption bands associated with

chitosan, glutaraldehyde crosslinking, and Zn-related interactions in the coating structure.

3. RESULTS AND DISCUSSION

Morphological Characterization (SEM)

Representative SEM images of the copper-supported chitosan–glutaraldehyde/zinc oxide coating are shown in **Figure 2.** At low magnification (50×; **Figure 2a**), the coating appears continuous and macroscopically uniform over the copper surface, with no obvious phase separation or large particulate agglomeration. At 500× (**Figure 2b)**, a polygonal crack-like pattern becomes visible, dividing the surface into sub-domains. At higher magnification (1500×; **Figure 2c**), the crack boundaries and compact intra-domain texture are more clearly resolved, indicating the formation of a dense crosslinked coating. The surface features are consistent with shrinkage during solvent evaporation and film consolidation in a crosslinked polysaccharide-based matrix. At 5000× **(Figure 2d),** micro-folds and fine micro-cracks were observed, whereas large ZnO agglomerates were not evident, suggesting that the inorganic phase remained well dispersed within the CS–GLA matrix.

Cross-sectional SEM images (**Figure 2e,f**) further show that the coating remained continuous and adhered intimately to the Cu substrate, with no obvious interfacial delamination. Although shallow cracks are visible in the outer region of the coating, they do not appear to propagate throughout the full thickness, and the inner layer remains cohesive. This observation suggests that the crack features are localized surface phenomena rather than indicators of complete structural failure. Such shallow crack networks may facilitate electrolyte access to the outer layer and increase the effective interfacial contact area, thereby contributing to ion-transport pathways during cyclic voltammetric measurements. At the same time, the preserved cohesion of the inner coating supports stable attachment to the Cu substrate, which is favorable for reproducible electrochemical response.

In the higher-magnification cross-sectional region (**Figure 2f**), the local coating thickness was approximately 27.3 μm. The broader low-magnification cross section (**Figure 2e**) showed a more irregular surface profile, indicating that the coating thickness was not fully uniform across the observed area, which is reasonable for a drop-cast system undergoing drying and shrinkage. Importantly, despite this local thickness variation, the cross-sectional images consistently show a continuous coating–substrate interface without large voids or film detachment.

Overall, the SEM observations indicate that the crosslinked chitosan matrix accommodated ZnO without obvious large-scale aggregation and maintained good interfacial contact with the copper support. This morphological uniformity is relevant to the electrochemical results, since a more homogeneous interfacial structure is expected to promote more uniform charge-transfer pathways and contribute to the reproducibility of the cyclic voltammetric response. These observations are consistent with previous reports showing that glutaraldehyde crosslinking can improve the structural stability and integrity of chitosan-based materials. [19,20] The absence of obvious large ZnO clusters further supports effective filler dispersion within the coating, which is also consistent with reported ZnO-containing chitosan composite systems. [24] Such structural features are favorable for reproducible cyclic voltammetric response and cycling stability.

Elemental Composition (EDS)

Area-averaged energy-dispersive X-ray spectroscopy (EDS) collected at 15 kV confirmed the presence of Zn, O, and Cu in the analyzed region of interest (**Figure 3a**). The Zn and O signals support the incorporation of Zn-containing inorganic domains within the coating, whereas the Cu signal is attributed to the underlying substrate. In addition, Na, Cl, Mg, and Si were detected in the analyzed region, which may reflect local surface residues, measurement geometry, and the semi-quantitative nature of standardless EDS analysis. Therefore, the EDS data are interpreted primarily in terms of elemental presence and spatial distribution rather than absolute bulk composition.

Elemental maps (**Figure 3b**) show that Zn- and O-related signals are distributed across the analyzed coating region without obvious large-scale segregation, supporting the interpretation that Zn-containing domains were immobilized within the CS–GLA network. This distribution is consistent with the compact, crack-bounded morphology observed by SEM and agrees with previous reports on ZnO/polymer composite systems[24]. Because EDS is semi-quantitative and sensitive to local sampling conditions, the present results are discussed mainly in terms of elemental distribution rather than absolute composition.

Taken together, the SEM and EDS observations indicate that the coating is structurally compact, compositionally distributed over the Cu surface, and well adhered to the substrate. These features are relevant to the electrochemical results, as a more uniform interfacial structure is expected to support stable ion-access pathways and reproducible cyclic voltammetric behavior.

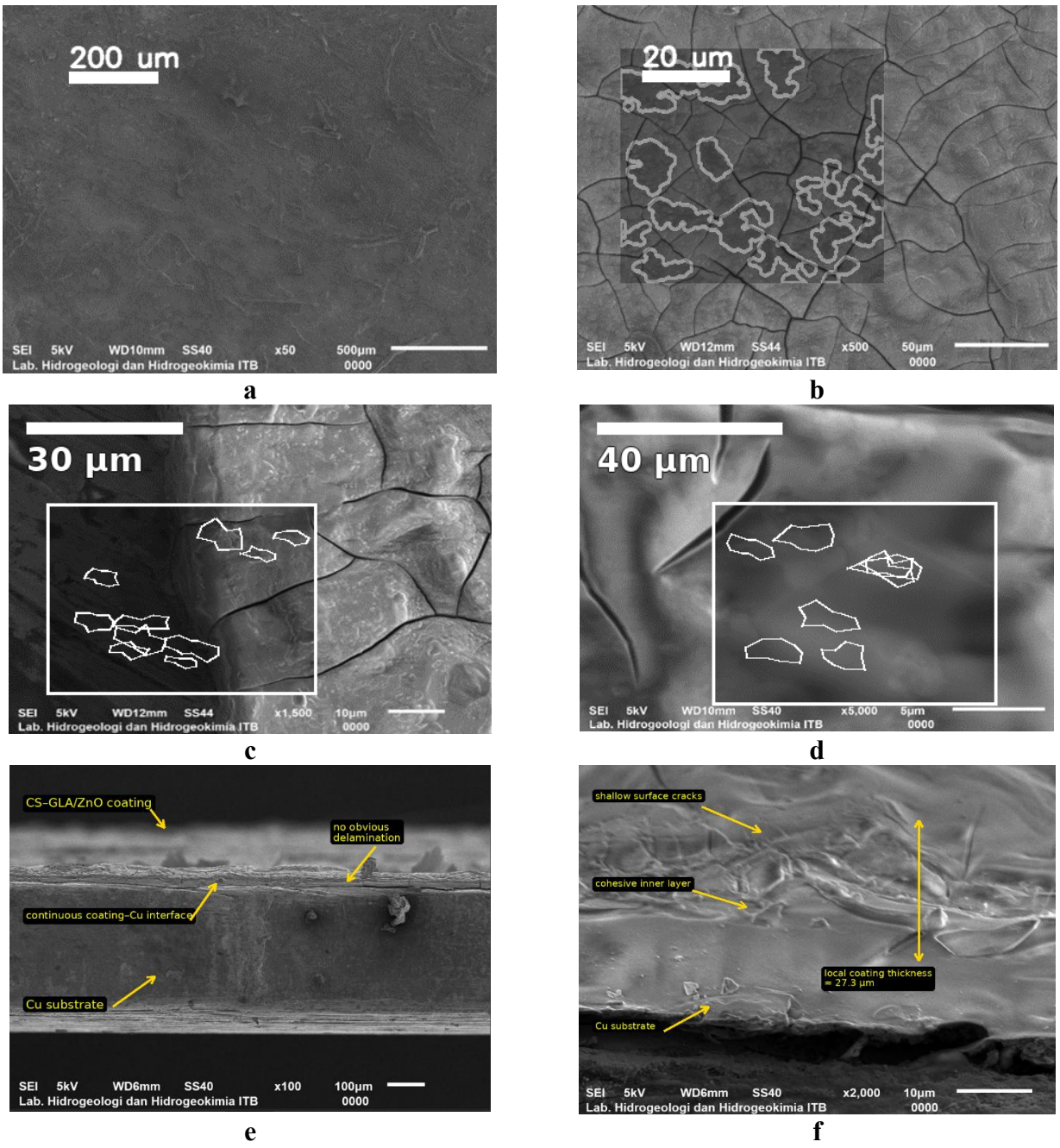

Figure 2. SEM micrographs of the copper-supported CS–GLA/ZnO coating: (a) 50× top view showing a continuous and macroscopically uniform surface; (b) 500× image showing a polygonal crack-like network; (c) 1500× image showing crack boundaries and compact intra-domain texture; (d) 5000× image showing micro-folds and fine micro-cracks without obvious large ZnO agglomerates; (e) 100× cross-sectional overview showing the CS–GLA/ZnO coating on Cu, a continuous coating–Cu interface, and no obvious delamination; (f) 2000× cross-sectional detail showing shallow surface cracks, a cohesive inner layer, and a local coating thickness of approximately 27.3 µm

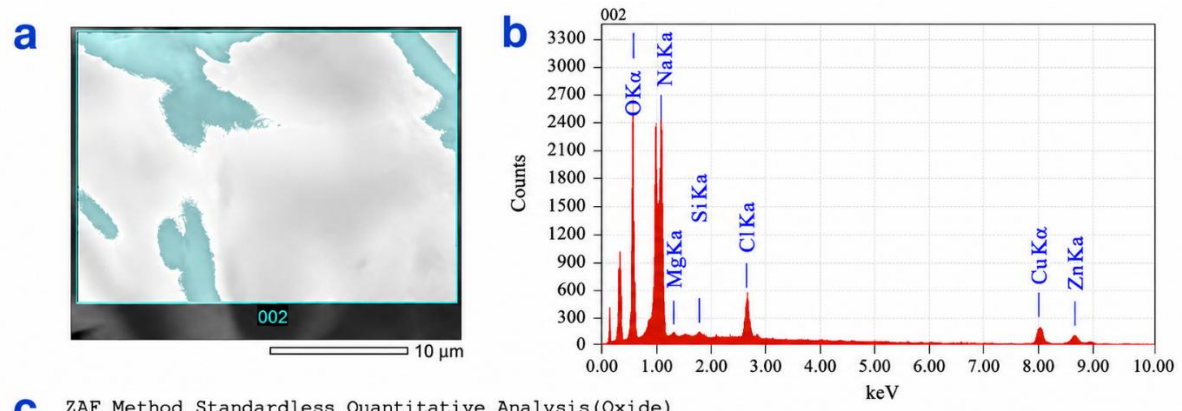

c

ZAF Method Standardless Quantitative Analysis(Oxide)
Fitting Coefficient : 0.2475
Total Oxide : 24.0

Element	(keV)	Mass%	Sigma	Mol%	Compound	Mass%	Cation	K
		20.12						
Na K	1.041	19.12	0.49	28.35	Na2O	25.77	15.53	15.0442
Mg K	1.253	0.47	0.14	1.33	MgO	0.78	0.36	0.2884
Si K	1.739	0.52	0.15	1.25	SiO2	1.10	0.34	0.5220
Cl K	2.621	7.08	0.15	13.62	Cl	7.08	0.00	10.6145
Cu K	8.040	30.99	1.14	33.26	CuO	38.79	9.11	43.6714
Zn K	8.630	21.27	1.12	22.19	ZnO	26.47	6.08	29.8596
Total		100.00		100.00		100.00	31.42	

Figure 3. (a) SEM image showing the analyzed region of interest (ROI; blue box); (b) EDS spectrum collected at 15 kV, showing prominent O, Na, Cu, and Zn signals together with minor Mg, Si, and Cl contributions; (c) standardless ZAF oxide-based semi-quantitative analysis of the same ROI. The data indicate the presence of Zn- and O-containing domains within the coating together with Cu from the substrate, while the relative elemental percentages should be interpreted cautiously because EDS is semi-quantitative and sensitive to local sampling conditions.

FTIR: Crosslinking and ZnO Coordination

The FTIR spectra of CS, GLA, CS–GLA, and CS–GLA/ZnO (**Figure 4**) support a dual stabilization mechanism in the coating, namely (i) covalent Schiff-base crosslinking within the chitosan matrix and (ii) Zn-related coordination within the organic–inorganic network. In the spectrum of pure GLA, the aldehydic C=O stretching band appears at approximately 1725 cm^{-1}, whereas in CS–GLA this band is no longer evident and a new absorption band emerges at 1625–1629 cm^{-1}, which is assigned to C=N stretching of the Schiff base. This spectral evolution is consistent with the reaction between the aldehyde groups of GLA and the amino groups of chitosan, suggesting the formation of imine linkages through the proposed crosslinking pathway shown in Eq. (1).

$$2CS\text{–}NH_2 + OHC\text{–}(CH_2)_3\text{–}CHO \rightarrow CS\text{–}N{=}CH\text{–}(CH_2)_3\text{–}CH{=}N\text{–}CS + 2H_2O \quad (1)$$

The Zn-related interaction in the composite can be schematically represented as follows:

$$CS\text{–}GLA\ (O/N\ donor\ sites) + ZnO \rightleftharpoons CS\text{–}GLA\cdots ZnO\ nanocomposite \quad (2)$$

Table 1. FTIR band assignments for CS, GLA, CS–GLA, and CS–GLA/ZnO nanocomposites

Sample	Peak position (cm^{-1})	Functional group	Assignment/vibration type
Chitosan (CS)	~3439	–OH/–NH_2 stretching	Hydrogen-bonded hydroxyl and amine vibrations
	~1603	–NH_2 bending	Primary amine deformation
	1154, 1027	C–O–C / C–O stretching	Ether and alcohol vibrations
Glutaraldehyde (GLA)	~1725	C=O (free aldehyde)	Aldehyde carbonyl stretching
CS–GLA	1625–1629	C=N (Schiff base)	Imine stretching due to crosslink formation
	—	1725 band absent	Consumption of aldehyde groups after crosslinking

CS–GLA/ZnO	~3417	–OH/–NH stretching	Strengthened hydrogen bonding and/or Zn-related interaction
	~1603	N–H bending	Modified amine-related contribution in the chitosan framework
	~617, ~462 (± ~750)	Zn–O and Zn-related coordination	Zn–O / Zn–N or related metal–ligand interaction modes
	1154, 1027; ~918	Polysaccharide framework bands	Retained chitosan backbone vibrations

Upon incorporation of ZnO, the CS–GLA/ZnO spectrum retains the major polysaccharide bands while showing additional changes in both the high- and low-wavenumber regions. The broad –OH/–NH stretching envelope shifts slightly from approximately 3439 cm^{-1} in CS to around 3417 cm^{-1} in CS–GLA/ZnO, suggesting strengthened hydrogen bonding and/or coordination interactions in the composite network. The band near 1603 cm^{-1} remains visible and is associated with N–H bending contributions in the modified chitosan framework. In the lower-wavenumber region, bands at approximately 617 and 462 cm^{-1}, together with a weak shoulder near 750 cm^{-1}, are attributed to Zn–O and Zn-related coordination modes, indicating interaction between Zn-containing domains and donor sites in the CS–GLA matrix. Meanwhile, the characteristic polysaccharide bands at 1154 and 1027 cm^{-1}, together with the feature near 918 cm^{-1}, remain present, indicating that the main chitosan backbone is preserved after crosslinking and ZnO incorporation.

Taken together, these spectral changes indicate that the coating structure is stabilized not only by imine crosslinks but also by Zn-related interactions within the organic–inorganic network. The disappearance of the aldehyde C=O band together with the appearance of the C=N band provides direct evidence of Schiff-base formation, whereas the low-wavenumber Zn-related bands support immobilization of Zn-containing domains within the crosslinked matrix. This dual stabilization is important for the electrode interface because it helps consolidate the chitosan network, improves structural cohesion, and promotes better retention of the inorganic phase within the coating. In combination with the SEM/EDS results, the FTIR analysis supports the formation of a compact and integrated coating architecture that is favorable for stable and reproducible cyclic voltammetric behavior. These chemical interactions are expected to strengthen the integrity of the coating and support stable interfacial behavior during electrochemical cycling.

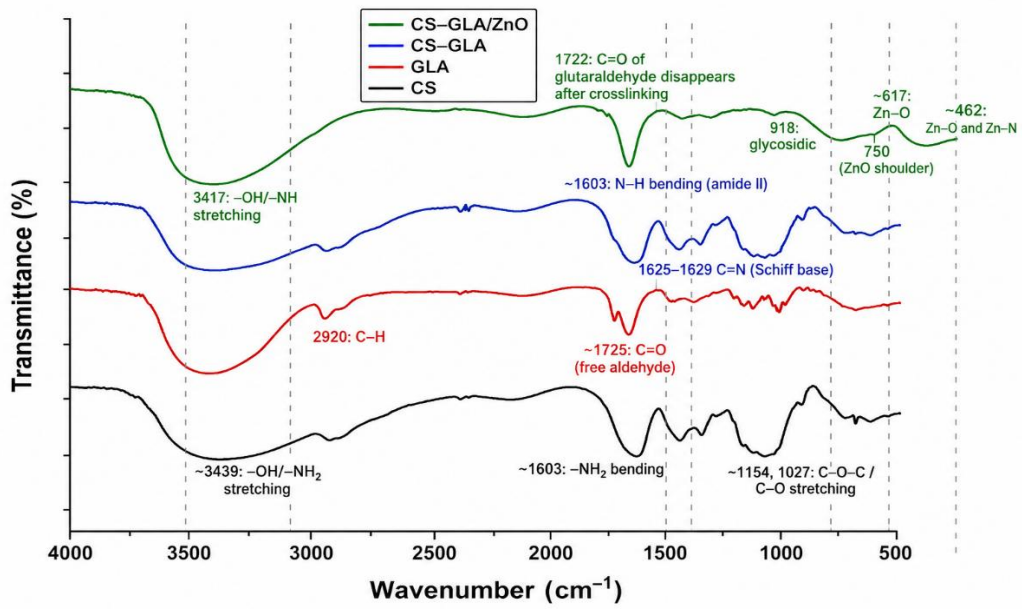

Figure 4. FTIR spectra of pure chitosan (CS), pure glutaraldehyde (GLA), CS–GLA, and CS–GLA/ZnO. Dashed lines indicate the main spectral changes associated with crosslinking and Zn-related interaction, including the disappearance of the aldehyde C=O band (~1725 cm^{-1}), the appearance of the Schiff-base C=N band (1625–1629 cm^{-1}), and Zn-related bands in the low-wavenumber region (~617 and ~462 cm^{-1}, with a weak shoulder near ~750 cm^{-1})

Cyclic Voltammetry of Cu|CS–GLA/ZnO Electrodes in PBS and Ferricyanide: Scan-Rate Dependence and Reversibility

The cyclic voltammetric responses of the Cu|CS–GLA/ZnO electrode were evaluated in 0.1 M phosphate-buffered saline (PBS, pH 7.0) and in 0.01 M $K_3[Fe(CN)_6]$/0.10 M KCl as a redox-probe electrolyte (**Figure 5**). In PBS, the voltammograms exhibited broadened anodic and cathodic features with peak separations (ΔE_p) in the range of 0.33–0.42 V and I_{pa} / $|I_{pc}|$ values below unity in most cases (**Table 2a**), indicating quasi-reversible electron transfer with additional resistive contributions associated with the polymer-coated interface [26]. By contrast, the ferricyanide system showed sharper redox features and generally more balanced anodic and cathodic responses, with ΔE_p values of 0.17–0.45 V and $I_{pa}/|I_{pc}|$ values closer to unity, particularly at 75–100 mV s^{-1} (**Table 2b**). This behavior indicates more efficient interfacial charge transfer in ferricyanide than in PBS.

$$Fe(CN)_6^{3-} + e \rightleftharpoons Fe(CN)_6^{4-} \quad (3)$$

For both electrolyte systems, the measured ΔE_p values remained substantially larger than the theoretical reversible limit of 59 mV for a one-electron process at 25 °C, indicating that the present responses are not ideally reversible. In the ferricyanide system, the electrochemical analysis was interpreted using the conventional one-electron assumption (n=1) for the $Fe(CN)_6^{3-/4-}$ couple. The formal potential, calculated as $E^{0'}=(E_{pa}+E_{pc})/2$, was used as a comparative reference for the electrode interface. Overall, the near-unity current ratio observed in ferricyanide at higher scan rates suggests a more balanced redox process, whereas the broader peaks and larger distortion in PBS are consistent with slower ion/electron transport through the coating and additional ohmic effects [26].

Scan-rate dependence and transport regime

To further evaluate how the electrode response evolved with scan rate, the cyclic voltammograms obtained in PBS and ferricyanide were compared as shown in **Figure 5**, and the corresponding electrochemical parameters are listed in **Tables 2a and 2b**. The voltammetric response of the Cu|CS–GLA/ZnO electrode changed systematically with scan rate in both electrolytes. In both media, the peak currents increased with scan rate, while the peak separation (ΔE_p) remained relatively large. This behavior is characteristic of quasi-reversible interfacial electron transfer rather than ideal reversible behavior.[41] In PBS, the voltammograms remained relatively broad, with ΔE_p values of 0.33–0.42 V and I_{pa} /$|I_{pc}|$ below unity in most cases, indicating quasi-reversible behavior with additional resistive contributions from the coating/electrolyte interface. In ferricyanide, the voltammograms were sharper and the anodic and cathodic currents became more balanced, especially at 75–100 mV s^{-1}, as reflected by I_{pa} /$|I_{pc}|$ values closer to unity. These features indicate improved interfacial charge transfer in ferricyanide relative to PBS under the present experimental conditions.

Table 2. Effect of scan rate (25–100 mV s^{-1}) on the cyclic voltammetric response of Cu|CS–GLA/ZnO electrodes (A=0.90 cm^2). (a) In 0.1 M PBS (pH 7.0), ΔE_p = 0.33–0.42 V and $I_{pa}/|I_{pc}|$ = 0.70–0.99 indicate quasi-reversible behavior with additional resistive contributions.

Scan rate (mV s^{-1})	I_{pa} (mA)	I_{pc} (mA)	$\lvert I_{pa} / I_{pc}\rvert$	E_{pa} (V)	E_{pc} (V)	ΔE_p (V)	E^0 (V)
25	2.10	-3.00	0.70	-0.12	-0.45	0.33	-0.29
50	2.40	-3.10	0.81	0.17	-0.25	0.42	-0.04
75	2.40	-3.12	0.77	0.17	-0.24	0.41	-0.04
100	2.40	-2.44	0.99	0.15	-0.20	0.35	-0.03

(b) In 0.01 M $K_3[Fe(CN)_6]$/0.10 M KCl, ΔE_p =0.17–0.45 V and $I_{pa}/|I_{pc}|$= 0.62–1.06 indicate improved charge balance and sharper redox response relative to PBS, with the most balanced behavior observed at 75–100 mV s^{-1}

Scan rate (mV s^{-1})	I_{pa} (mA)	I_{pc} (mA)	$\lvert I_{pa} / I_{pc}\rvert$	E_{pa} (V)	E_{pc} (V)	ΔE_p (V)	E^0 (V)
25	2.20	-2.50	0.88	0.03	-0.25	0.28	-0.11
50	2.30	-3.70	0.62	-0.40	-0.75	0.35	-0.58
75	2.40	-2.35	1.06	0.10	-0.35	0.45	-0.13
100	2.48	-2.50	0.92	-0.20	-0.37	0.17	-0.29

Table 3. Linearity of I_p versus √ν from least-squares fitting (n = 4 scan rates). In PBS, the moderate anodic linearity and weak cathodic linearity indicate additional resistive and interfacial effects within the coating. In ferricyanide, the excellent anodic linearity ($R^2 \approx 0.996$) is consistent with diffusion-controlled anodic transport, whereas the weaker cathodic linearity suggests non-ideal reverse-process behavior. Accordingly, diffusion-coefficient estimation was based on the ferricyanide anodic response

System	Peak	Slope (mA $s^{1/2}$ $V^{-1/2}$)	Intercept (mA)	R^2
PBS (0.1 M, pH 7.0)	I_{pa}	1.832	1.880	0.691
PBS (0.1 M, pH 7.0)	I_{pc}	-2.825	3.601	0.359
$K_3[Fe(CN)_6]$/0.10 M KCl	I_{pa}	1.782	1.912	0.996
$K_3[Fe(CN)_6]$/0.10 M KCl	I_{pc}	-2.004	3.249	0.047

Table 4. Apparent diffusion coefficients of Cu|CS–GLA/ZnO electrodes estimated from the Randles–Ševčík relationship in the ferricyanide electrolyte system

Electrolyte system	Peak used	Basis of estimation	Assumed (n)	Apparent (D) range (cm^2 s^{-1})	Interpretation
0.01 M $K_3[Fe(CN)_6]$/ 0.10 M KCl	I_{pa}	CV/ Randles–Ševčík	1	10^{-5} – 10^{-6}	apparent electrochemical transport parameter; anodic response is consistent with stronger diffusion-controlled behavior

To further examine the transport regime, the peak currents were analyzed as a function of the square root of scan rate ($v^{1/2}$) according to the Randles–Ševčík relationship for diffusion-controlled electrochemical processes at 25 °C [41]

$$I_p = 2.69 \times 10^5 \, n^{3/2} \, ACD^{1/2} \, v^{1/2} \quad (4)$$

where I_p is the peak current (A), n is the number of transferred electrons, A is the electroactive area (cm^2), C is the bulk concentration of the redox species (mol cm^{-3}), D is the apparent diffusion coefficient (cm^2 s^{-1}), and v is the scan rate (V s^{-1}). The coefficient 2.69×10^5 applies at 25 °C. In this work, the ferricyanide system was interpreted using the conventional one-electron assumption ($n=1$), and the cathodic peak currents were evaluated using their absolute values.

To evaluate the transport regime more quantitatively, the relationship between peak current and the square root of scan rate was analyzed by least-squares fitting, and the corresponding results are summarized in **Table 3**. In the ferricyanide electrolyte, the anodic peak current showed excellent linearity with $v^{1/2}$ (R^2=0.996), which is consistent with predominantly diffusion-controlled anodic transport under the investigated conditions. However, the cathodic response in ferricyanide showed much weaker linearity (R^2=0.047), indicating that the reverse process was influenced by additional interfacial factors beyond ideal semi-infinite diffusion. In PBS, the anodic response showed only moderate linearity (R^2=0.691), while the cathodic response was considerably weaker (R^2=0.359). These findings indicate that charge transport in PBS is more strongly affected by coating resistance, interfacial polarization, and non-ideal ion-access behavior within the CS–GLA/ZnO layer.[26]

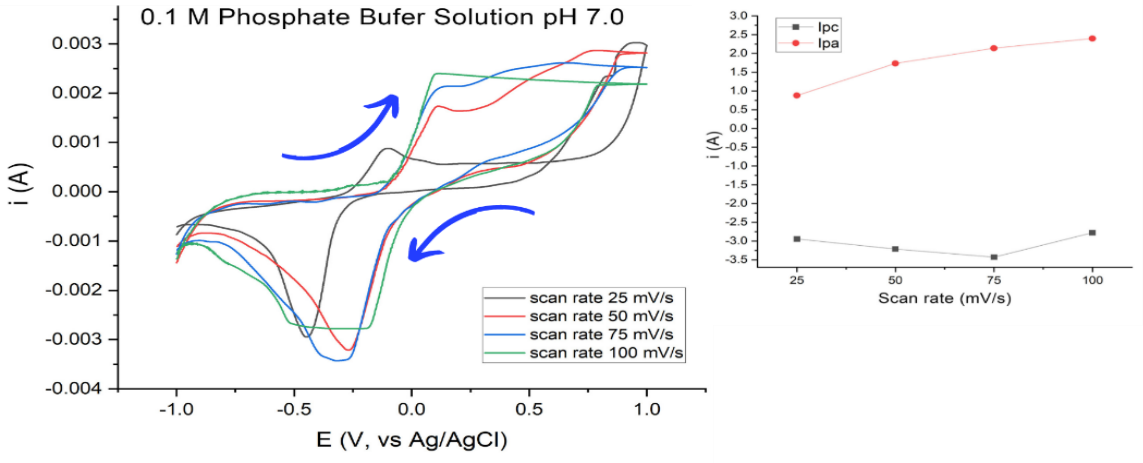

a

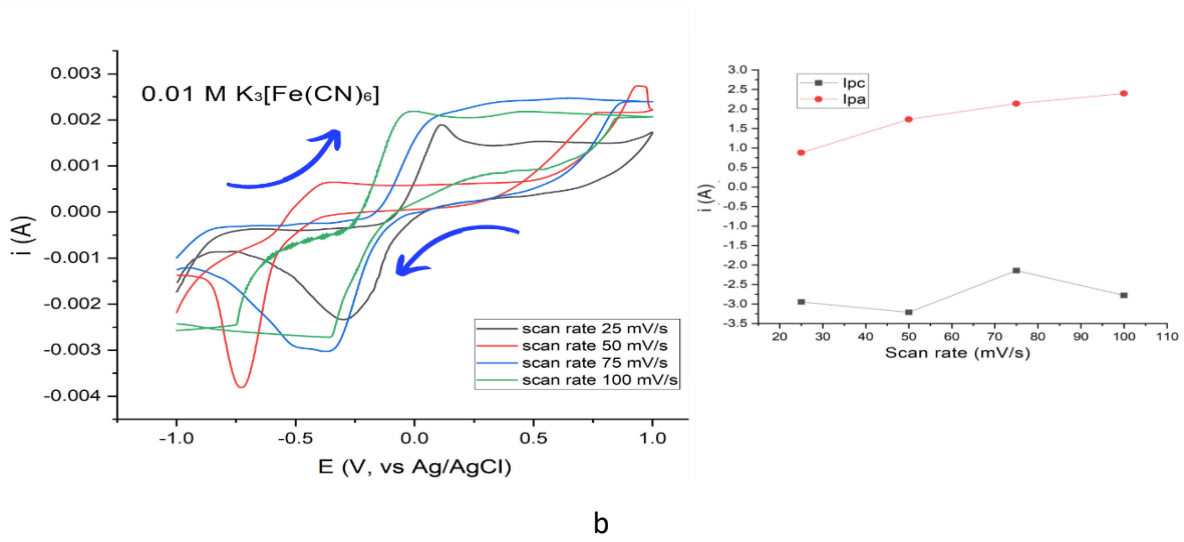

Figure 5. Cyclic voltammograms of Cu|CS–GLA/ZnO electrodes recorded at scan rates of 25–100 mV s^{-1} in (a) 0.1 M phosphate-buffered saline (PBS, pH 7.0) and (b) 0.01 M $K_3[Fe(CN)_6]$/0.10 M KCl, together with the corresponding scan-rate dependence of anodic and cathodic peak currents. In PBS, the broader redox features and larger ΔE_p values indicate quasi-reversible behavior with additional resistive contributions from the coating/electrolyte interface. In ferricyanide, the sharper redox response and current ratios closer to unity indicate improved interfacial charge transfer, particularly at 75–100 mV s^{-1}

The apparent diffusion coefficient was estimated only for the ferricyanide system because the $Fe(CN)_6^{3-/4-}$ couple provides a well-defined redox probe with known bulk concentration and n=1. The estimated values are summarized in **Table 4**. The apparent diffusion coefficients fall in the 10^{-5}–10^{-6} cm^2 s^{-1} range and should be regarded as apparent electrochemical transport parameters rather than intrinsic diffusivities, because the system departs from ideal reversibility and includes contributions from interfacial resistance and coating structure.[41] This interpretation is also consistent with the SEM observations: the shallow crack-like surface topology may facilitate electrolyte access to the outer coating region, whereas the cohesive cross-sectional structure helps maintain interfacial continuity during electrochemical cycling.

At 75–100 mV s^{-1}, the voltammetric parameters extracted from **Figure 5**, and summarized in **Tables 2a** and **2b,** show that $I_{pa}/|I_{pc}|$ became closer to unity in both media, while ΔE_p remained within 0.35–0.45 V in PBS and 0.17–0.45 V in ferricyanide. Under the present experimental conditions, this scan-rate range provided the most balanced response with reduced peak distortion. Consistent with **Table 3**, PBS showed larger ΔEp, weaker current linearity, and stronger resistive effects, whereas ferricyanide exhibited sharper redox features, more balanced current ratios, and excellent anodic linearity, indicating more favorable interfacial charge transfer.

Reproducibility and electrode-to-electrode variation (n = 10)

The reproducibility of the Cu|CS–GLA/ZnO electrode was evaluated using ten independently prepared electrodes (n=10) fabricated under the same preparation procedure. **Figure 6** shows the overlaid cyclic voltammograms obtained under representative conditions in PBS and ferricyanide, while the quantitative reproducibility parameters are summarized in **Table 5**. The anodic peak current (I_{pa}) was used as the primary response parameter, and the results are reported as mean ± standard deviation (SD) together with relative standard deviation (RSD).

As shown in **Figure 6a**, the PBS responses recorded at 50 mV s^{-1} exhibited a broader spread among independently prepared electrodes. Under this condition, the mean anodic peak current was I_{pa} =1.640 ± 0.088 mA, corresponding to an RSD of 5.4%. By contrast, the ferricyanide responses recorded at 75 mV s^{-1} in **Figure 6b** were more tightly clustered. Under this condition, the mean anodic peak current was I_{pa} = 2.109 ± 0.076 mA, corresponding to an RSD of 3.6%. Thus, the ferricyanide system showed lower electrode-to-electrode variability than PBS, indicating a more consistent voltammetric response under the present conditions.

The broader spread observed in PBS is consistent with the larger ΔE_p, lower $I_{pa}/|I_{pc}|$, and weaker scan-rate linearity discussed in the previous section, all of which indicate stronger resistive and interfacial constraints in this medium. By contrast, ferricyanide provided sharper redox features, more

balanced peak-current ratios, and more consistent anodic responses, in agreement with its more favorable interfacial charge-transfer behavior. The improved reproducibility in ferricyanide is consistent with the more favorable charge-transfer characteristics of the $Fe(CN)_6^{3-/4-}$ redox couple, the supporting-electrolyte ionic strength, and reduced ohmic and migration effects [26,41].

Any remaining spread is likely associated with micro-heterogeneity in coating thickness and tortuosity, as well as local differences in crosslink density and nanoparticle distribution across the Cu surface. This interpretation is consistent with the SEM/EDS observations, which suggest that the coating is generally compact and well distributed but still subject to local microstructural variation. Therefore, tighter control of drop-casting volume, crosslinking conditions, and ZnO dispersion may further reduce electrode-to-electrode variance, consistent with the known influence of glutaraldehyde crosslinking and ZnO incorporation on the stability and uniformity of chitosan-based composite materials.[19]

Overall, the reproducibility results confirm that the Cu|CS–GLA/ZnO coating provides a stable and reasonably consistent electrochemical interface across independently prepared electrodes. The tighter clustering of the ferricyanide responses in **Figure 6b** and the lower RSD value further support the use of this medium for comparative electrochemical characterization of the present coating under the investigated conditions.

Table 5. Reproducibility of Cu|CS–GLA/ZnO electrodes across ten independently prepared electrodes (n=10), expressed as mean anodic peak current (I_{pa}) ± standard deviation (SD) and relative standard deviation (RSD) under representative conditions in PBS and ferricyanide

Electrolyte system	Scan rate (mV s^{-1})	Response parameter	Mean ± SD (mA)	RSD (%)
0.1 M PBS (pH 7.0)	50	I_{pa}	(1.640 ± 0.088)	5.4
0.01 M $K_3[Fe(CN)_6]$/0.10 M KCl	75	I_{pa}	(2.109 ± 0.076)	3.6

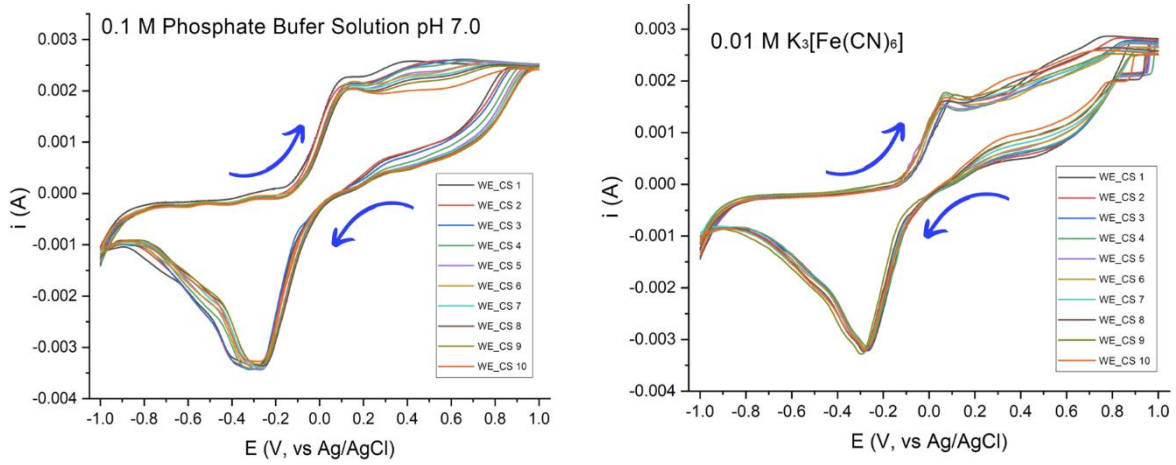

a **b**

Figure 6. Reproducibility of Cu|CS–GLA/ZnO electrodes across ten independently prepared electrodes (n=10). Overlaid cyclic voltammograms were recorded in (a) 0.1 M phosphate-buffered saline (PBS, pH 7.0) at 50 mV s^{-1} and (b) 0.01 M $K_3[Fe(CN)_6]$/0.10 M KCl at 75 mV s^{-1}. Quantitative reproducibility parameters (mean I_{pa} ± SD and RSD) are provided in the text and **Table 5**

Electrochemical stability under repeated cycling

The electrochemical stability of the Cu|CS–GLA/ZnO electrode under repeated cycling was evaluated by recording cyclic voltammograms from −1.0 to +1.0 V versus Ag/AgCl over 5, 10, and 15 consecutive cycles in PBS and ferricyanide media (**Figure** 7). In both electrolytes, the overall voltammetric profiles were generally retained during repeated cycling, indicating that the coating remained electrochemically active and structurally stable within the investigated potential window.

In 0.1 M phosphate-buffered saline (PBS, pH 7.0) at 75 mV s^{-1}, the voltammograms showed only minor variations in peak shape and current intensity over 5, 10, and 15 cycles. No pronounced shift in the overall response pattern was observed, indicating that the Cu|CS–GLA/ZnO coating maintained a reasonably

stable interfacial behavior during repeated cycling in PBS. In 0.01 M $K_3[Fe(CN)_6]$/0.10 M KCl at 50 mV s^{-1}, a more noticeable change was observed during the early cycles, followed by a more stable voltammetric pattern upon further cycling. This behavior is consistent with an initial conditioning or wetting process of the electrode/coating interface before reaching a relatively steady response.

The observed cycling stability is consistent with the structural features identified in the previous sections. SEM/EDS showed a compact coating morphology with no obvious large ZnO agglomeration and good attachment to the Cu substrate, while FTIR supported stabilization of the coating through Schiff-base crosslinking and Zn-related interactions within the CS–GLA/ZnO network. Together, these chemical and structural characteristics likely help maintain Zn-containing domains within the coating and preserve interfacial continuity during repeated potential cycling.[26]

Overall, **Figure 7** indicates that the Cu|CS–GLA/ZnO coating can maintain its voltammetric response over at least 15 cycles without evidence of severe signal deterioration or interfacial failure under the present experimental conditions. These results support the stability of the coating for comparative electrochemical measurements and suggest that further control of crosslink density, ZnO dispersion, and film thickness may help further reduce drift and improve long-term cycling consistency. Although using a different electrode modifier and target analyte, recent work has similarly emphasized the importance of modified electrode interfaces in improving nonenzymatic electrochemical sensing performance.[42]

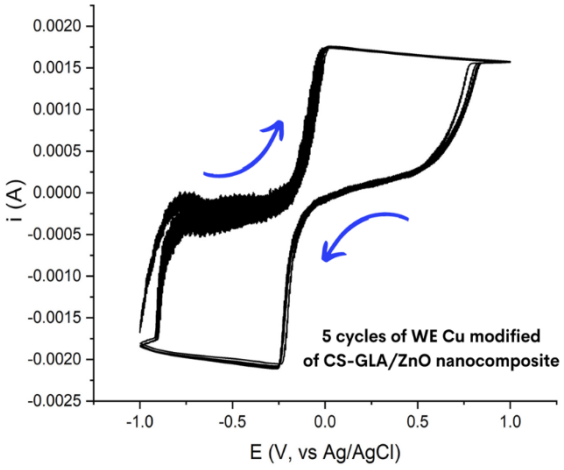

a

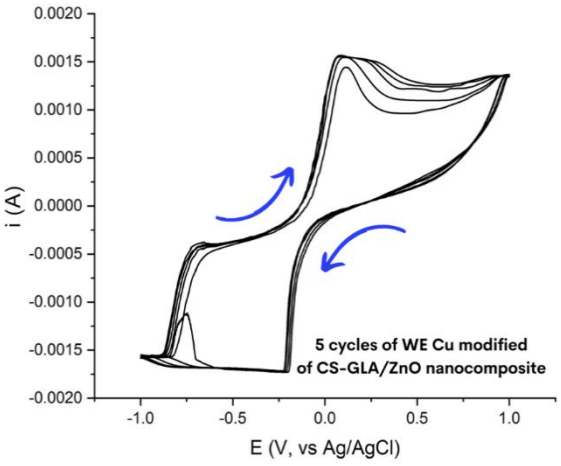

b

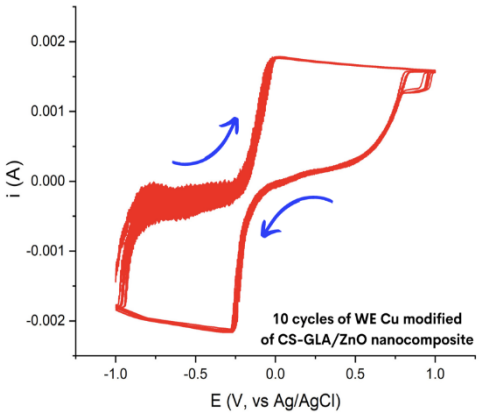

c

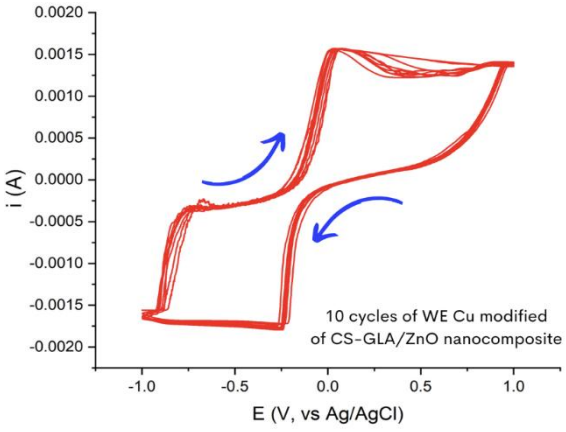

d

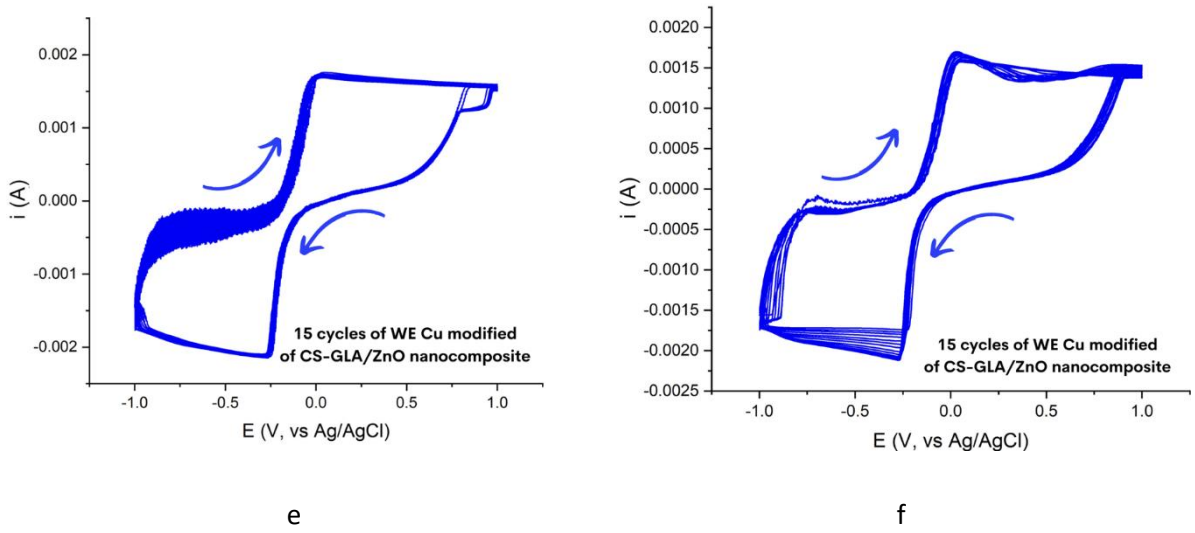

e f

Figure 7. Electrochemical stability of Cu|CS–GLA/ZnO-modified Cu electrodes during repeated cycling. Cyclic voltammograms were recorded from −1.0 to +1.0 V versus Ag/AgCl for 5, 10, and 15 consecutive cycles in (a, c, e) 0.1 M phosphate-buffered saline (PBS, pH 7.0) at 75 mV s^{-1} and (b, d, f) 0.01 M $K_3[Fe(CN)_6]$/0.10 M KCl at 50 mV s^{-1}. The results show retention of the overall voltammetric profile with only minor variation in PBS and an initial conditioning effect, followed by a more stable response in ferricyanide

4. CONCLUSIONS

A copper-supported crosslinked chitosan–glutaraldehyde/zinc oxide coating was successfully prepared and shown to provide a stable electrochemical interface. FTIR confirmed Schiff-base crosslinking and Zn-related interactions within the organic–inorganic network, while SEM/EDS indicated a compact coating with cohesive cross-sectional structure, good attachment to Cu, and distributed Zn-containing domains without obvious large-scale agglomeration. Electrochemically, the Cu|CS–GLA/ZnO electrode exhibited quasi-reversible behavior in both PBS and ferricyanide, with ferricyanide giving sharper redox features, current ratios closer to unity, and stronger anodic linearity with $\nu^{1/2}$. The apparent diffusion coefficient estimated from the ferricyanide anodic response was on the order of 10^{-5}–10^{-6} cm^2 s^{-1}. Reproducibility across ten independently prepared electrodes was acceptable, with lower variability in ferricyanide than in PBS, and the overall voltammetric profile was retained over 15 cycles. These results demonstrate that the Cu|CS–GLA/ZnO coating provides a stable and reasonably reproducible chitosan-based electrochemical interface, representing a promising platform for future sensing applications.

ACKNOWLEDGMENTS

The authors gratefully acknowledge financial support from the Ministry of Research, Technology, and Higher Education of the Republic of Indonesia through the DRTPM PTM and PFR research grant schemes awarded to the AM Research Group (Master Contract No. 125/C3/DT.05.00/PL/2025; Derivative Contract No. 8010/LL4/PG/2025; 04/PKS/LPPM-UNJANI/VI/2025; and 05/PKS/LPPM-UNJANI/VI/2025).

REFERENCES

1. Azizi SN, Ghasemi S, Amiripour F. Nickel/P Nanozeolite Modified Electrode: A New Sensor for the Detection of Formaldehyde. *Sens Actuators B Chem*. 2016;227:1-10. doi:10.1016/j.snb.2015.11.142
2. Zhou ZL, Kang TF, Zhang Y, Cheng SY. Electrochemical Sensor For Formaldehyde based on Pt-Pd Nanoparticles and A Nafion-Modified Glassy Carbon Electrode. *Microchimica Acta*. 2009;164(1-2):133-138. doi:10.1007/s00604-008-0046-x
3. Momeni S, Sedaghati F. CuO/Cu2O nanoparticles: A simple and Green Synthesis, Characterization and Their Electrocatalytic Performance Toward Formaldehyde Oxidation. *Microchemical Journal*. 2018;143:64-71. doi:10.1016/j.microc.2018.07.035
4. Rahman MM. Efficient Formaldehyde Sensor Development Based On Cu-Codoped Zno Nanomaterial By an Electrochemical Approach. *Sens Actuators B Chem*. 2020;305:127541. doi:10.1016/j.snb.2019.127541
5. Hosseini SR, Raoof JB, Ghasemi S, Gholami Z. Pd-Cu/poly(o-anisidine) Nanocomposite as an Efficient Catalyst for Formaldehyde Oxidation. *Mater Res Bull*. 2016;80:107-119. doi:10.1016/j.materresbull.2016.03.040
6. Hajilari F, Farhadi K, Eskandari H, Allahnouri F. Application of Cu/porous Silicon

Nanocomposite Screen Printed Sensor for The Determination of Formaldehyde. *Electrochim Acta*. 2020;355:1-8. 17. doi:10.1016/j.electacta.2020.136751
7. Zhang H, Yun S, Song L, Zhang Y, Zhao Y. The Preparation and Characterization of Chitin and Chitosan under Large-Scale Submerged Fermentation Level using Shrimp By-Products As Substrate. *Int J Biol Macromol*. 2017;96:334-339. doi:10.1016/j.ijbiomac.2016.12.017
8. Vedula SS, Yadav GD. Chitosan-based Membranes Preparation and Applications: Challenges and opportunities. *Journal of the Indian Chemical Society*. 2021;98(2):1-14. doi:10.1016/j.jics.2021.100017
9. Saputra HA, Andreas. Chitosan and its biomedical applications: A review. *Next Materials*. 2025;9. doi:10.1016/j.nxmate.2025.101270
10. Karim MM, Lasker T, Sahin AZ, Hossain S, Saputra HA. *Low-Cost Production of Chitosan Biopolymer from Seafood Waste: Extraction and Physiochemical Characterization*. Vol 12.; 2023.
11. Liu CY, Chou YC, Tsai JH, Huang TM, Chen JZ, Yeh YC. Tyrosinase/Chitosan/Reduced Graphene Oxide Modified Screen-Printed Carbon Electrode for Sensitive and Interference-Free Detection of Dopamine. *Applied Sciences (Switzerland)*. 2019;9(4):1-9. doi:10.3390/app9040622
12. Sun C, Zou Y, Wang D, Geng Z, Xu W, Liu F, Cao J. Construction of chitosan-Zn-Based Electrochemical Biosensing Platform for Rapid and Accurate Assay of Actin. *Sensors (Switzerland)*. 2018;18(6):1-13. doi:10.3390/s18061865
13. Eljali A, Nainggolan I, Hashim S, Nasution TI, Wahab NZA. Fabrication of Chitosan-Polyethylene Oxide Polymeric Thin Film using Electrochemical Deposition for Detection of Volatile Organic Compounds. *Key Eng Mater*. 2017;744 744 KE:359-363. doi:10.4028/www.scientific.net/KEM.744.359
14. Sanjari AJ, Asghari M. A Review on Chitosan Utilization in Membrane Synthesis. *ChemBioEng Reviews*. 2016;3(3):134-158. doi:10.1002/cben.201500020
15. Application of Chitosan/Fe_3O_4 Nanocomposite as Biosensor. *Letters in Applied NanoBioScience*. 2021;10(3):2438-2445. doi:10.33263/lianbs103.24382445
16. Liu P, Yin L, Qi X. Application of Glassy Carbon Electrode Modified with Chitosan and ZnO Nanoparticles as Enzymatic Glucose Biosensor. *Int J Electrochem Sci*. 2020;15:5821-5832. doi:10.20964/2020.06.67
Figiela M, Wysokowski M, Galinski M, Jesionowski T, Stepniak I. Synthesis and Characterization of Novel Copper Oxide-Chitosan Nanocomposites for Non-Enzymatic Glucose Sensing. *Sens Actuators B Chem*. 2018;272:296-307. doi:10.1016/j.snb.2018.05.173
18. Liu L, Pan Z. Properties of Hydrophilic Chitosan/Polysulfone Nanofibrous Filtration Membrane. *J Eng Fiber Fabr*. 2014;9(1):76-86. doi:10.1177/155892501400900109
19. Beppu MM, Vieira RS, Aimoli CG, Santana CC. Crosslinking of Chitosan Membranes using Glutaraldehyde: Effect on Ion Permeability and Water Absorption. *J Memb Sci*. 2007;301(1-2):126-130. doi:10.1016/j.memsci.2007.06.015
20. Galan J, Trilleras J, Zapata PA, Arana VA, Grande-Tovar CD. Optimization of Chitosan Glutaraldehyde-Crosslinked Beads for Reactive Blue 4 Anionic Dye Removal Using a Surface Response Methodology. 2021;11(2):1-20. doi:10.3390/life11020085
21. Bui TH, Lee W, Jeon SB, Kim KW, Lee Y. Enhanced Gold(III) Adsorption using Glutaraldehyde-Crosslinked Chitosan Beads: Effect of Crosslinking Degree on Adsorption Selectivity, Capacity, and Mechanism. *Sep Purif Technol*. 2020;248:1-12. doi:10.1016/j.seppur.2020.116989
22. Wang ZL. Zinc Oxide Nanostructures: Growth, Properties and Applications. *Journal of Physics Condensed Matter*. 2004;16(25):1-31. doi:10.1088/0953-8984/16/25/R01
23. Saisa, Agusnar H, Alfian Z, Nainggolan I. Polymer of Chitosan with ZnO Addition to Optimize High Responsivity and Sensitivity in Sensor Film. *AIP Conf Proc*. 2020;2267(September):1-8. doi:10.1063/5.0016439
24. Reghioua A, Barkat D, Jawad A, Abdulhameed AS, Rangabhashiyam S, Khan MR, AlOthhman ZA. Magnetic Chitosan-Glutaraldehyde/Zinc Oxide/Fe3O4 Nanocomposite: Optimization and Adsorptive Mechanism of Remazol Brilliant Blue R Dye Removal. *J Polym Environ*. 2021:1-16. doi:10.21203/rs.3.rs-450675/v1
25. Qiu B, Xu X feng, Deng R hui, Xia G qing, Shang X fu, Zhou P hu. Construction of chitosan/ZnO nanocomposite film by in situ precipitation. *Int J Biol Macromol*. 2019;122:82-87. doi:10.1016/j.ijbiomac.2018.10.084

26. Wang J. *Analytical Electrochemistry*. 2nd ed. New York: John Wiley & Sons; 2001. doi:10.5860/choice.38-5590
27. Elgrishi N, Rountree KJ, McCarthy BD, Rountree ES, Eisenhart TT, Dempsey JL. A Practical Beginner's Guide to Cyclic Voltammetry. *J Chem Educ*. 2018;95(2):197-206. doi:10.1021/acs.jchemed.7b00361
28. Kundu M, Rajesh, Krishnan P, Gajjala S. Comparative Studies of Screen-Printed Electrode Based Electrochemical Biosensor with the Optical Biosensor for Formaldehyde Detection in Corn. *Food Bioproc Tech*. 2021;14(4):726-738. doi:10.1007/s11947-021-02604-3
29. Chou TC, Chang CC, Yu HL, Yu WY, Dong CL, Velasco-Vélez JJ, Chuang CH, Chen LC, Lee JF, Chen JM, Wu HL. Controlling the Oxidation State of the Cu Electrode and Reaction Intermediates for Electrochemical CO_2 Reduction to Ethylene. *J Am Chem Soc*. 2020;142(6):2857-2867. doi:10.1021/jacs.9b11126
30. Rivaldi MH, Rizky A, Hardian A, Murniati A. Study of Aluminum-Copper Electrodes for Chromium and Chemical Oxygen Demand Removal from Tannery Wastewater by Electrocoagulation. *Jurnal Riset Kimia*. 2025;16(1):33-44. doi:10.25077/jrk.v16i1.744
31. Farshchi F, Hasanzadeh M, Feyziazar M, Saadati A, Hassanpour S. Electropolymerization of Chitosan in The Presence Of Cunps on The Surface of A Copper Electrode: An Advanced Nanocomposite for The Determination of Mefenamic Acid and Indomethacin in Human Plasma Samples and Prevention of Drug Poisoning. *Analytical Methods*. 2020;12(9):1212-1217. doi:10.1039/c9ay02789k
32. Murniati A, Buchari B, Gandasasmita S, Nurachman Z, Hardian A, Triani D. Immobilization of Crude Polyphenol Oxidase Extracts from Apples on Polypyrrole as a Membrane for Phenol Removal. *Jurnal Kimia Sains dan Aplikasi*. 2021;24(2):62-69. doi:10.14710/jksa.24.2.62-69
33. Murniati A, Buchari B, Gandasasmita S, Nurachman Z. Synthesis and Characterization of Polypyrrole Polyphenol Oxidase (PPy/PPO) on Platinum Electrode. *Res J Pharm Biol Chem Sci*. 2012;3(4):1-10.
34. Murniati A, Buchari B, Gandasasmita S, Nurachman Z. Sintesis dan Karakterisasi Elektroda Kerja Kasa Baja Dengan Metode Voltammetri Siklik. 2012;13(3):210-215.
35. Vellingiri K, Deep A, Kim KH, Boukhvalov DW, Kumar P, Yao Q. The Sensitive Detection of Formaldehyde in Aqueous Media Using Zirconium-Based Metal Organic Frameworks. *Sens Actuators B Chem*. 2017;241:938-948. doi:10.1016/j.snb.2016.11.017
36. Kundu M, Bhardwaj H, Pandey MK, Krishnan P, Kotnala RK, Sumana G. Development of Electrochemical Biosensor based on CNT–Fe_3O_4 Nanocomposite to Determine Formaldehyde Adulteration in Orange Juice. *J Food Sci Technol*. 2019;56(4):1829-1840. doi:10.1007/s13197-019-03635-7
37. Murniati A, Nur IH, Gumelar N, Budiman S, Buchari B, Gandasasmita S, Nurachman Z. Evaluation of Scan Rate Influence on Cyclic Voltammograms of Copper Electrodes Coated with PS-CS-GA/ZnO Nanocomposite. *Jurnal Kartika Kimia*. 2024;7(1). doi:10.26874/jkk.v7i1.256
38. Aprillianti RN, Rahayu M, Hardian A, Murniati A. Effect of Polyethylene Glycol Concentration on the Structural and Mechanical Properties of Polysulfone-Based Membranes. *Journal of Chemistry and Environment*. October 2024:25-38. doi:10.56946/jce.v3i2.469
39. Murniati A, Shardi S, Fauzi I, Hardian A, Ibrahim RM, Buchari B, Gandasasmita S, Nurachman Z. Immobilization of Crude Polyphenol Oxidase Purple Eggplant Extract on Chitosan Membrane for Removal of Phenol Wastewater. European Chemical Bulletin. 2022;11(10):117-125. doi:10.31838/ecb/2022.11.10.016
40. Gunawan AF, Hardian A, Murniati A. Cyclic Voltammetry Study of the Influence of Concentration of K3[Fe(CN)6] and Glucose on Glassy Carbon Electrode. *ALCHEMY Jurnal Penelitian Kimia*. 2025;21(1):43-52. doi:10.20961/alchemy.21.1.87604.43-52
41. Bard AJ, Faulkner LR. *Electrochemical Methods: Fundamentals and Applications*. 2nd ed. New York: John Wiley & Sons; 2001. doi:10.1038/s41929-019-0277-8
42. Nisa U, Iswantini D, Ahmad SN, Mahat MM, Putra BR, Saskito DIB, Wahyuni WT. Nonenzymatic Sensor Based on Glassy Carbon Electrode Modified by Platinum Nanoparticles Decorated Reduced Graphene Oxide for Glucose Detection in Human Urine. *Jurnal Kimia Valensi*. 2024;10(2):215-228. doi:10.15408/jkv.v10i2.40035